Molecular Packing in Unsubstituted Semiconducting Phenylenevinylene Oligomer and Polymer

Paul F. van Hutten, Jurjen Wildeman, Auke Meetsma, and Georges Hadziioannou*

Contribution from the Department of Polymer Science and the Crystal Structure Centre of the Department of Chemical Physics, Materials Science Centre, University of Groningen, Nijenborgh 4, NL-9747 AG Groningen, The Netherlands

Received March 22, 1999

Abstract: *p*-Bis(*p*-styrylstyryl)benzene, $C_{38}H_{30}$, a five-ring phenylene−vinylene model compound for unsubstituted PPV, has been obtained in single-crystal form and the crystal structure has been resolved. The arrangement of the molecules is of the herringbone-type, and its characteristic dimensions correspond remarkably well to those of the structure proposed for PPV in 1986. This packing mode is entirely different from what has been found for substituted oligo(phenylenevinylene)s but similar to that observed in other types of conjugated oligomers without lateral substituents. Thin films of the unsubstituted oligomer show electroluminescence at a lower onset voltage and blue-shifted relative to substituted oligo(phenylenevinylene)s.

Introduction

The significant progress in both fundamental science and applications of conjugated polymers achieved during this decade has led to renewed interest in the solid-state properties of aromatic compounds. A considerable experimental and basic knowledge was gathered already during the 1960s and 1970s, much of which has been well documented in the authoritative book by Pope and Swenberg.[1]

Polymers, however, are distinct from small molecule substances in their mesoscale structure (this terminology will be used loosely here to cover a range of length scales between that of the chain segment and that of micrometers; it comprises supramolecular order and morphology). Even a single, well-defined polymer chain architecture may lead to a plethora of mesostructures, metastable in general, as a result of thermodynamic and hydrodynamic factors that are operative during the formation of the solid from the melt or from solution. Each property of the polymer solid will depend on its mesostructure to some degree. In retrospective, one finds that issues of local order and mesostructure have been largely bypassed in the work on conjugated polymers. In most of the early work, a direct relation between the physical property and the (idealized) chemical structure is sought. The presence of chemical defects in the polymer chain and the occurrence of intersegment interactions ("aggregate" behavior) have only recently been invoked to explain observations.

Unfortunately, the structure at the chain segment level is hard to characterize. This inaccessibility of polymer solids is one of the reasons that model compounds, well-defined oligomeric analogues of a polymer, have met increasing interest in the field of conjugated organics.[2] Because of the chemical purity and relatively low molecular mass, these model compounds are usually sufficiently crystalline to allow structural resolution by means of diffraction methods; often, single crystals can be obtained. This opens a way to interrelate changes of the molecular structure and changes of the solid-state structure (molecular conformation and packing), and to study the effect of both on the solid-state properties (optical and electrical characteristics). This information may help us understand the behavior of the analogous polymer.

The properties of oligomers may compare so favorably with that of the related polymer as to offset the disadvantage of a more tedious processing, e.g., vacuum deposition of the oligomer versus spin-coating of the polymer. The best-known example of this is sexithiophene, from which efficient thin-film field effect transistors have been manufactured.[3,4] Through chemical perfectioning, increasing the regularity of its chain architecture, the parent substituted polythiophene has now caught up in this area of application.[5] This case serves to illustrate that chemical synthesis plays a crucial, often overlooked, role.

This paper deals with the solid-state structure of oligo(phenylenevinylene)s (OPV) as model compounds for poly(phenylenevinylene) (PPV), a light-emitting polymer that has recently seen its first commercial applications. An early report on the spectroscopy of phenylenevinylene oligomers by Drefahl et al. dates back to 1970.[6] Most of the later studies, prompted by the interest in PPV, were also concerned with emission properties. Many of those studies employed the 3,5-di-*tert*-butylphenyl-end-capped compounds introduced by Schenk et al.[7] In our previous studies of PPV-analogous model compounds, we have presented the crystal structures of substituted five-ring oligomers,[8−10] their deposition as thin films, and their light

(1) Pope, M.; Swenberg, C. E. *Electronic Processes in Organic Crystals*; Clarendon Press: Oxford, UK, 1982.

(2) *Electronic Materials: The Oligomer Approach*; Müllen, K., Wegner, G., Eds.; Wiley-VCH: Weinheim, Germany, 1998.

(3) Garnier, F.; Yassar, A.; Hajlaoui, R.; Horowitz, G.; Deloffre, F.; Servet, B.; Ries, S.; Alnot, P. *J. Am. Chem. Soc.* **1993**, *115*, 8716−8721.

(4) Torsi, L.; Dodabalapur, A.; Lovinger, A. J.; Katz, H. E.; Ruel, R.; Davis, D. D.; Baldwin, K. W. *Chem. Mater.* **1995**, *7*, 2247−2251.

(5) Sirringhaus, H.; Tessler, N.; Friend, R. H. *Science* **1998**, *280*, 1741−1744.

(6) Drefahl, G.; Kühmstedt, R.; Oswald, H.; Hörhold, H.-H. *Makromol. Chem.* **1970**, *131*, 89−103.

(7) Schenk, R.; Gregorius, H.; Meerholz, K.; Heinze, J.; Müllen, K. *J. Am. Chem. Soc.* **1991**, *113*, 2634−2647.

(8) Gill, R. E.; Meetsma, A.; Hadziioannou, G. *Adv. Mater.* **1996**, *8*, 212−214.

10.1021/ja990934r CCC: $18.00
Published on Web 06/15/1999

Scheme 1. Possible Routes for the Synthesis of P_5V_4: (a) Wittig−Horner, (b) Heck, and (c) Siegrist

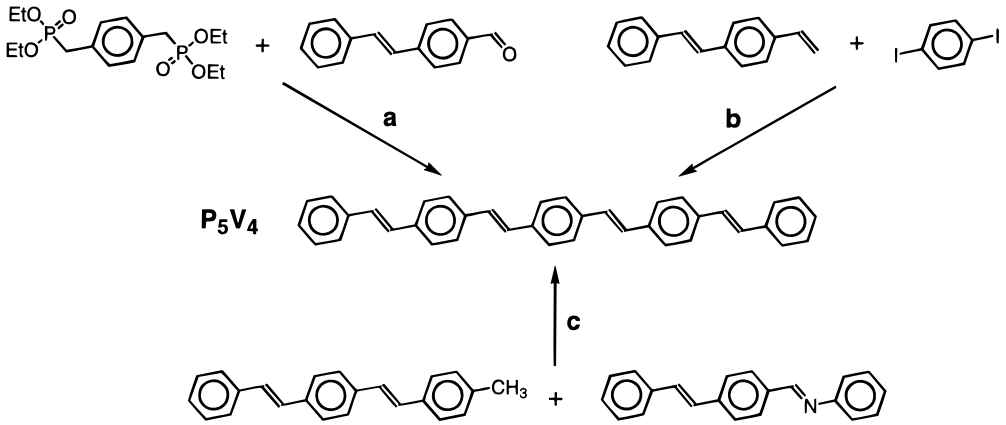

emission properties.[10−12] In this paper, we present our recent data on the crystal structure of the unsubstituted five-ring oligomer. The molecular arrangement in PPV is reviewed in the light of these new results.

For reasons of clarity, we introduce the notation P_5V_4 for the five-ring compound. Before, these oligomers were denoted OPV5s, while other authors have used 4PV or PV4, referring to the number of full phenylenevinylene repeat units.

Experimental Section

Synthesis. For the synthesis of *p*-bis(*p*-styrylstyryl)benzene (P_5V_4), three different methods of preparation have been applied: (a) the Wittig−Horner,[13] (b) the Heck,[14] and (c) the Siegrist reaction[15] (Scheme 1). The yields were found to vary from 40% in the Siegrist reaction to 70% in the Heck reaction.

After isolation, the crude P_5V_4 was purified successively by high-vacuum sublimation (10^{-6} mbar, 320−340 °C) and recrystallization from *trans*-stilbene. The crystallization of the oligomer was performed in a U-shaped glass tube, provided with a sintered P-3 glass filter in the middle. The oligomer was dissolved in *trans*-stilbene by placing a mixture of the two compounds (approximately 2:100 (w/w)) on one side of the filter in the U-tube and heating it to 285 °C (metal bath). The solution was cooled to 245 °C, after which thin plate-shaped crystals of P_5V_4 separated within 2 h. The crystals were isolated by filtering the hot solvent through the glass filter (the U tube was tilted and pressure was applied on the side containing the crystals). After further cooling (below 100 °C), the crystals were washed with toluene and subsequently with ether (below 30 °C). The crystals were put under vacuum on paraffin flakes (10^{-6} mbar, 125 °C) for one night in a drying pistol. MS *m*/*e* (rel intensity) 486 (M^+, 100), 243 ($M^+/2$, 15). Anal. Calcd for $C_{38}H_{30}$: C, 93.79; H, 6.21. Found: C, 93.41; H, 6.17.

Thermal Characterization. Differential scanning calorimetry (DSC) measurements were performed on a Perkin-Elmer 7 series thermal analyzer system at heating and cooling rates of 10 °C min^{-1}. The temperature scale was calibrated against zinc (T_m = 419.6 °C). For Thermogravimetric analysis (TGA) in a nitrogen atmosphere, a Perkin-Elmer TGA7 was used.

X-ray Crystallography. Yellow colored, very thin plate-shaped crystals were obtained by recrystallization as described above under Synthesis. To overcome the problem of weak intensities obtained on a conventional four-circle diffractometer, data collection was made by means of CCD area detector systems. The first set was obtained at 220 K by courtesy of Nonius BV who made their demonstration KappaCCD diffractometer and detector system available to us. The second data set was obtained at room temperature on a Bruker SMART 1000 CCD diffractometer system, courtesy of Bruker Analytical X-ray Systems.

(a) Data Set 1. A crystal of approximate dimensions 0.02 × 0.15 × 0.21 mm^3 was glued on top of a glass fiber and transferred into the cold nitrogen stream of the low-temperature unit mounted on a Nonius KappaCCD diffractometer[16] (55 kV, 32 mA, monochromatic Mo Kα radiation). Four sets of data were collected at various κ, θ, and ϕ offsets. Frames of 1° in ω exposed for 2 × 75 s were collected, filling the Ewald sphere. The data collection strategy was calculated by using a Nonius collect package. The unit cell was refined on all data and identified as monoclinic. The space group $P2_1/a$ was derived from the systematic extinctions. Data processing and scaling was carried out with DENZO-SMN.[17] Scaling includes corrections for decay and absorption and reduction of data intensities to F_o^2. The structure was solved by DIRDIF[18] employing automated vector-search rotation functions (ORIENT), followed by reciprocal space translation functions (TRACOR), taking an 11-carbon-atoms end-fragment skeleton as a starting fragment. The model was accomplished by direct methods applied to difference structure factors. Neutral atom scattering factors and anomalous dispersion corrections were taken from *International Tables for Crystallography*.[19] A subsequent difference Fourier synthesis resulted in the location of some of the hydrogen atoms, but in view of the unfavorable data-to-parameter ratio (1765 reflections with $F_o \geq 4.0\sigma(F_o)$), all hydrogen atoms were ultimately refined riding on their carrier atoms with their positions calculated by using sp^2 hybridization at the C atom as appropriate, with $U_{iso} = cU_{equiv}$, where $c = 1.2$ and values of U_{equiv} are related to the atoms to which the H atoms are bonded. Refinement on F^2 was carried out by full-matrix least-squares techniques[20] with the observance criterion $F^2 \geq 0$ applied. The final difference Fourier map showed no peaks having chemical meaning above the general background.

(b) Data Set 2. A crystal with dimensions 0.03 × 0.09 × 0.22 mm^3 mounted on a glass fiber was aligned on a Bruker SMART 1000 CCD diffractometer.[21] Intensity measurements were performed with Mo Kα

(9) Gill, R. E.; Van Hutten, P. F.; Meetsma, A.; Hadziioannou, G. *Chem. Mater.* **1996**, *8*, 1341−1346.
(10) Van Hutten, P. F.; Krasnikov, V. V.; Brouwer, H.-J.; Hadziioannou, G. *Chem. Phys.* **1999**, *241*, 139−154.
(11) Brouwer, H. J.; Krasnikov, V. V.; Pham, T. A.; Gill, R. E.; Van Hutten, P. F.; Hadziioannou, G. *Chem. Phys.* **1998**, *227*, 65−74.
(12) Brouwer, H.-J.; Krasnikov, V. V.; Pham, T.-A.; Gill, R. E.; Hadziioannou, G. *Appl. Phys. Lett.* **1998**, *73*, 708−710.
(13) Boutagy, J.; Thomas, R. *Chem. Rev.* **1974**, *74*, 87−99.
(14) Heck, R. F. In *Organic Reactions*; Dauben, W. G., et al., Eds.; John Wiley & Sons Inc.: New York, 1982; Vol. 27, Chapter 2.
(15) Siegrist, A. E.; Liechti, P.; Meyer, H. R.; Weber, K. *Helv. Chim. Acta* **1969**, *52*, 2521−2554.
(16) *Enraf-Nonius KappaCCD Software*; Enraf-Nonius Delft, Scientific Instruments Division: Delft, The Netherlands, 1998.
(17) Otwinowski, Z.; Minor, W. In *Methods in Enzymology*; Carter, C. W., Jr., Sweet, R. M., Eds.; Academic Press: New York, 1997; Vol. 276, pp 307−326.
(18) Beurskens, P. T.; Beurskens, G.; Bosman, W. P.; De Gelder, R.; García-Granda, S.; Gould, R. O.; Israël, R.; Smits, J. M. M. *The DIRDIF-97 program system*; Crystallography Laboratory, University of Nijmegen: Nijmegen, The Netherlands, 1997.
(19) *International Tables for Crystallography*; Wilson, A. J. C., Ed.; Kluwer Academic Publishers: Dordrecht, The Netherlands, 1992; Vol. C.
(20) Sheldrick, G. M. *SHELX-97, Program for the Solution and Refinement of Crystal Structures*; University of Göttingen: Göttingen, Germany, 1997.

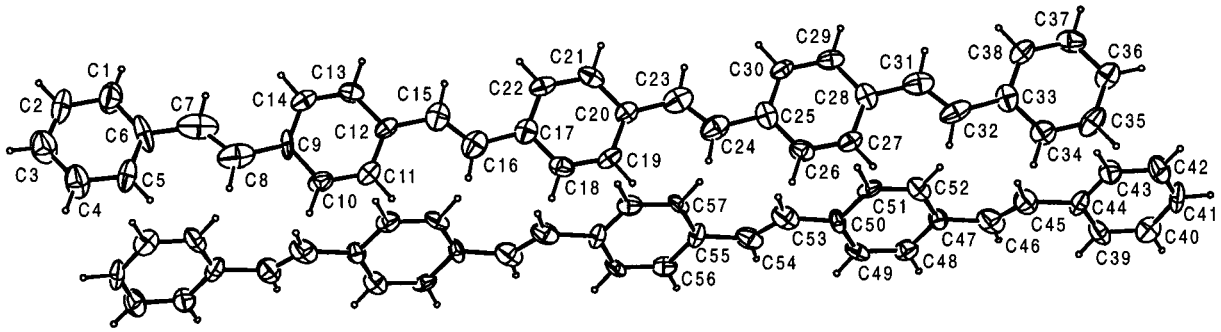

Figure 1. ORTEP drawing of the non-hydrogen atoms of P_5V_4 with the atom labeling scheme (50% probability ellipsoids). The hydrogen atoms are drawn with an arbitrary radius. (Data collected at 220 K.)

radiation from a sealed tube. Generator settings were 50 kV, 40 mA. SMART was used for preliminary determination of the cell constants and data collection control. A sphere of data was collected by a combination of three sets of exposures (frames). Each set had a different ϕ angle for the crystal and each exposure covered a range of 0.3° in ω. A total of 1800 frames were collected with an exposure time of 120 s per frame. The program SAINT was used for data integration. The program suite SXTL was used for space group determination (XPREP), structure solution (XS), and refinement (XL).

Crystal data and numerical details on data collection and refinement are given in Table 1. Since the structure resolved from data set 1 had a somewhat higher accuracy than that found from data set 2, details of the former study are available as Supporting Information. Figure 1 shows an ORTEP representation.

Electroluminescence. Light-emitting diodes were realized in a standard configuration ITO/OPV/Al. Thin films of P_5V_4 were deposited onto an ITO (indium−tin oxide) electrode on glass by vacuum sublimation from a molybdenum boat at approximately 350 °C and at a deposition rate of 2−4 Å s^{-1}. The ITO-covered glass slides had been cleaned using a procedure based on rinsing in deionized water and ultrasonic rinsing in polar and nonpolar organic solvents. The cathode consisted of a 100 nm aluminum layer deposited directly onto the organic layer at a pressure of 2×10^{-6} mbar. The cathode was deposited through a shadow mask to produce diodes with active areas of 7×10^{-2} cm^2. Photo- and electroluminescence spectra of the thin-film devices were recorded on a SLM-Aminco SPF500C or a Perkin-Elmer LS-50B spectrofluorometer. Current−voltage ($I-V$) and luminance−voltage ($L-V$) measurements were performed in a dry-nitrogen atmosphere glovebox to avoid exposure to ambient oxygen and water. $I-V$ characterization of the devices was performed with a Keithley 236 SMU operating in pulsed mode to minimize heating of the device. $L-V$ characteristics and external quantum efficiencies (photon/electron) were measured with the device mounted on an integrating sphere (LabSphere). Light intensities were measured with a calibrated photodiode, using the Keithley 236 SMU and a Stanford Research SR400 photon-counting device.

Table 1. Crystallographic and Experimental Data for P_5V_4

	data set	
	1	2
	crystal data	
formula	$C_{38}H_{30}$	
formula weight (g mol^{-1})	486.66	
crystal system	monoclinic	monoclinic
space group, no.	$P2_1/a$, 14	$P2_1/a$, 14
a (Å)	16.072(1)	16.115(4)
b (Å)	7.538(1)	7.6191(16)
c (Å)	32.914(2)	32.989(7)
β (deg)	103.349(3)	103.088(9)
V (Å^3)	3879.8(6)	3945.3(14)
Formula_Z	6	6
Space Group_Z	4	4
F(000) (electrons)	1548	1548
D_{calc} (g cm^{-3})	1.250	1.229
μ(Mo Kα) (cm^{-1})	0.69	0.69
crystal size (mm^3)	0.02 × 0.15 × 0.21	0.03 × 0.09 × 0.22
	data collection	
diffractometer system	Nonius KappaCCD	Bruker SMART 1000
T (K)	220	293(2)
wavelength	0.71073	0.71073
θ range: min, max (deg)	1.91, 23.28	0.63, 23.25
no. of data collected	6082	26345
no. of unique data	5580	5662
no. of data with $F_o \geq 4.0\sigma(F_o)$	1765	1273
	structure and refinement	
no. of reflcns, n ($F_o^2 > 0$)	5580	5662
no. of parameters refined, p	514	514
$R(F)$[a]	0.0917	0.1322
$wR(F^2)$[b]	0.2632	0.3501
S(GoF)[c]	0.882	1.598
residual ρ (e Å^{-3})	−0.33, 0.57(6)	−0.345, 0.742
max shift/σ, final cycle	<0.001	<0.001

[a] $R(F) = \sum||F_o| - |F_c||/\sum|F_o|$, for $F_o \geq 4.0\sigma(F_o)$. [b] $wR(F^2) = \{\sum[w(F_o^2 - F_c^2)^2]/\sum[w(F_o^2)^2]\}^{1/2}$, for $F_o^2 > 0$. [c] $S(\mathrm{GoF}) = \{\sum[w(F_o^2 - F_c^2)^2]/(n-p)\}^{1/2}$.

Results and Discussion

Purification and Crystallization of P_5V_4. The primary reason for substituting PPV with hydrocarbon side chains is to render the polymer soluble in common organic solvents at room temperature. Still, these substituents result in noticeable changes in the electronic properties of the molecules in solution, and in more dramatic changes in the behavior of the solid. For five-ring oligomers, it was found necessary to attach two rather long alkyl(oxy) side chains to attain fair solubility.[8] (Actually, branched chains are preferable since linear side chains longer than C_8 crystallize among themselves.) Whereas the chemical synthesis of P_5V_4 can be achieved through well-known methodologies (as outlined in the Experimental Section), the limited solubility obviously severely hampers the purification and the preparation of single crystals. We have succeeded by carrying out these steps at high temperature, using the solute-analogous compound *trans*-stilbene as the high-boiling solvent. Since *trans*-stilbene has a melting point of 125 °C, crystallization must occur well above this temperature (the boiling point of stilbene is 305 °C). To minimize contamination, as much of the stilbene as possible was removed at high temperature, before proceeding to the washing steps at lower temperatures.

Thermal Behavior. Successful processing of P_5V_4 at 285 °C for recrystallization requires that the compound is stable at this temperature. This was checked and confirmed by TGA

(21) *SMART, SAINT and SHELXTL, Area Detector Control and Integration Software*; Bruker Analytical X-ray Instruments. Inc.: Madison, WI, 1999.

Table 2. DSC Data for P_5V_4, Corresponding to the Curves in Figure 3[a]

scan[b]	T_{min} (°C)	T_{max} (°C)	$T_{endo,1}$ (°C)	$\Delta H_{endo,1}$ (J/g)	$T_{endo,2}$ (°C)	$\Delta H_{endo,2}$ (J/g)	$T_{endo,3}$ (°C)	$\Delta H_{endo,3}$ (J/g)	$T_{exo,3}$ (°C)	$T_{exo,2}$ (°C)	$\Delta H_{exo,2}$ (J/g)	$T_{exo,1}$ (°C)	$\Delta H_{exo,1}$ (J/g)
A, 1st cycle	250	450	384.4	29.6	415.4	64.5	433.2	3.8	393.8[c]	384	−49.5[c]	347.9	−11.7
A, 2nd up	250	450	361.7	9.8	394.0	—[d]	400	44.9[d]					
B, 1st cycle	25	400	385.7	30.5								380.4	−28.5
B, 2nd up	25	400	385.5	29.3									
C, 1st cycle	300	420	381.2	27.5	412.0	63.1				408.6	−52.3	369.3	−19.6
C, 2nd up	300	420	376.0	22.1	409.0	52.1							

[a] The T_{endo} and T_{exo} values listed are peak temperatures. [b] The first cycle includes heating from T_{min} to T_{max} and cooling to T_{min}, all at a rate of 10 °C min^{-1}. [c] Exotherms 3 and 2 are not well-separated; the combined enthalpy is listed as $\Delta H_{exo,2}$. [d] Endotherms 2 and 3 are not well-separated; the combined enthalpy is listed as $\Delta H_{endo,3}$.

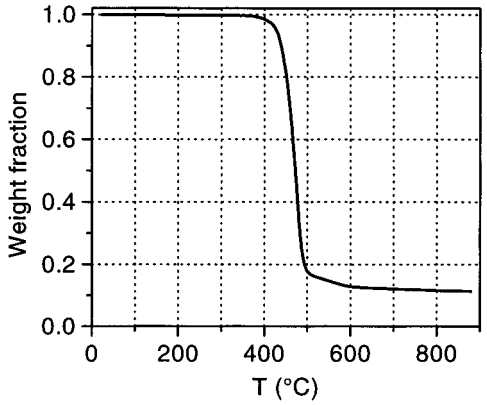

Figure 2. TGA curve of P_5V_4, recorded at a heating rate of 10 °C min^{-1}.

measurements (Figure 2). The solid does not lose weight at temperatures below 350 °C. In our opinion, the stability of P_5V_4 will not be modified by the presence of stilbene since the latter is a homologous compound.

The thermal behavior was investigated further by means of DSC experiments, using standard heating and cooling rates of 10 °C min^{-1}. In the scan shown in Figure 3A, the sample was heated to 450 °C. Three distinct endotherms were observed. The maximum temperature of 450 °C is obviously within the range of degradation according to the TGA results (Figure 2). Indeed, the subsequent cooling and heating scans clearly showed that chemical changes had occurred in the sample. Only 40% of the enthalpy input is returned in the exotherms.

To explore this further, two runs on fresh samples were conducted in which the up scan extended to just beyond the first and second endotherms, respectively. In the first run, the sample melts over the range 381−390 °C (Figure 3B). Cooling is started without pause at 400 °C, and crystallization is found to occur at a peak-to-peak supercooling of 5 °C and over a range of 6 °C, during which 93% of the enthalpy is recovered. The maximum temperature of 400 °C is just past the onset, at a few percent weight loss, of the TGA curve. That this is not a severe condition is demonstrated by a subsequent DSC up scan: the melting enthalpy is almost equal to that of the first up scan, and the shift of the endotherm to lower temperatures is within 0.5 °C.

In the next experiment, the up scan was stopped and the down scan started at 420 °C, after the complete appearance of the second endotherm (Figure 3C). Two exotherms appear during cooling. Of these two, the second one is broader and situated about 10 °C lower than the exotherm of the run shown in Figure 3B. Eighty percent of the enthalpy is recovered. The endotherms in the second up scan are shifted down by 3−5 °C and slightly broader than those in the first up scan. Some degradation has occurred, but it is far less severe than in the case of the experiment of Figure 3A.

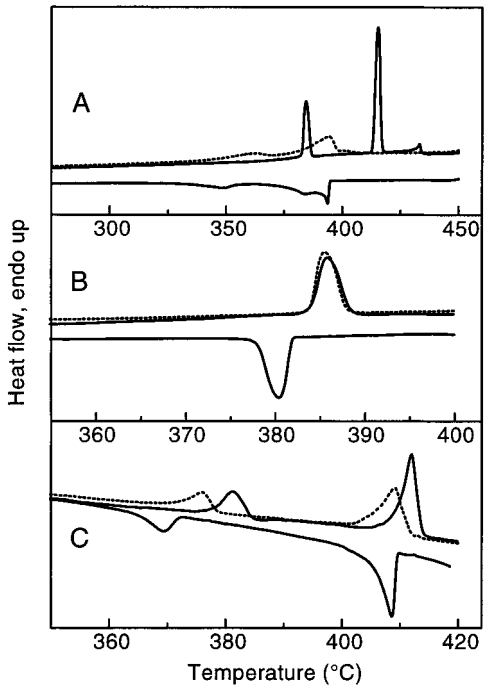

Figure 3. DSC thermograms of P_5V_4, recorded at heating and cooling rates of 10 °C min^{-1}. A, B, and C each contain a series of first heating and cooling (—) and second heating (· · ·) runs on fresh samples. The maximum temperature between the first heating and cooling runs was different in each case: A, 450 °C; B, 400 °C; and C, 420 °C.

DSC data are collected in Table 2. The three endotherms found below 440 °C suggest that P_5V_4 displays liquid-crystalline behavior, and that there are actually two distinct LC phases. The heat values associated with the endotherms lead us to hypothesize that these correspond to a crystal-to-smectic (C−S), a smectic-to-nematic (S−N), and a nematic-to-isotropic (N−I) transition, respectively. The high temperatures involved have so far prevented us from doing structural studies on these phases.

LC behavior has also been observed for α-sexithiophene around 310 °C.[22,23] At that temperature, the formation of the LC phase was found to compete with polymerization of the oligomer to polythiophene. Results similar to ours for P_5V_4 have been reported for oligo(*p*-phenylene)s, in particular *p*-sexiphenyl, by Baker et al.[24] The authors ascribe the three endotherms to C−C, C−S, and S−N transitions, respectively, with observation of the N−I transition being precluded by sample decomposition.

The Crystal Structure of Unsubstituted PPV: From Oligomer to Polymer. The analyses at 220 and 293 K lead to

(22) Taliani, C.; Zamboni, R.; Ruani, G.; Rossini, S.; Lazzaroni, R. *J. Mol. Electron.* **1990**, *6*, 225−226.

(23) Destri, S.; Mascherpa, M.; Porzio, W. *Adv. Mater.* **1993**, *5*, 43−45.

(24) Baker, K. N.; Fratini, A. V.; Resch, T.; Knachel, H. C.; Adams, W. W.; Socci, E. P.; Farmer, B. L. *Polymer* **1993**, *34*, 1571−1587.

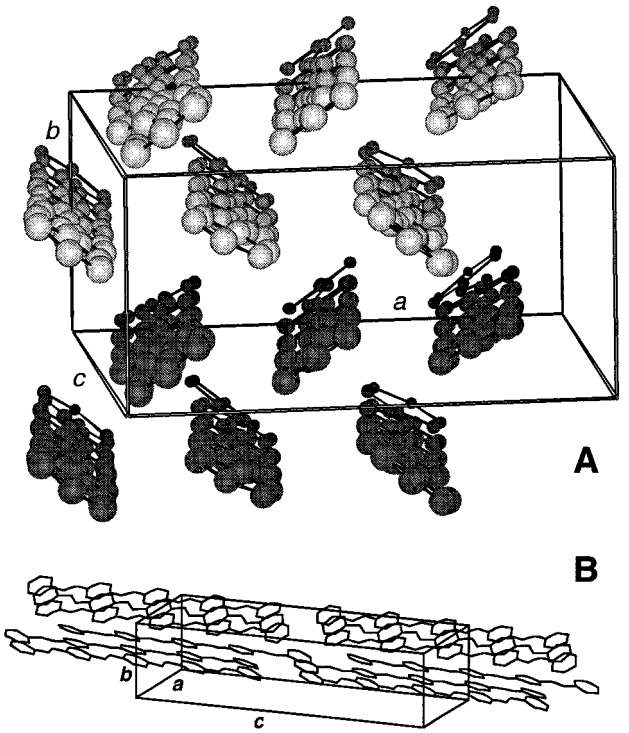

Figure 4. Packing arrangement of P_5V_4 in the crystal lattice. (A) View at a slight angle with respect to the long molecular axis; six molecules that occupy one unit cell are depicted in an identical shade of gray (the two sets of six molecules are *b*-axis neighbors). (B) Wireframe view almost perpendicular to the long axis (the two sets of six molecules are *c*-axis neighbors). H atoms have been omitted for clarity.

the same crystallographic and molecular structure (see next section for a discussion of the lattice expansion). The asymmetric unit of the cell contains one and a half molecules (Figure 1), which translates into a total of six molecules through the symmetry operations of the $P2_1/a$ space group. Two of these six molecules, as a matter of course, have a center of inversion. The six units are separated by normal van der Waals distances,[25] and no solvent-accessible voids were detected by the procedures implemented in the PLATON package used for geometry calculations.[26] A number of views on the unit cell are shown in Figures 4−7.

The packing arrangement is of the "herringbone" type: the molecular axes are parallel but the molecular planes in adjacent layers are inclined with respect to each other. Since the P_5V_4 molecules are neither all identical nor entirely planar (see below), the inclination is not uniquely defined; between the (more planar) centrosymmetric molecules it is ca. 71° (Figure 5). Herringbone is a usual packing pattern of long conjugated molecules without substituents, oligomers as well as polymers: polyacetylene (see, e.g., ref 27 and references therein), poly(*p*-phenylene),[28] polythiophene,[29] and PPV[30] have this arrangement. Among the common polymers, polyethylene[31] is an example. In polymers with herringbone packing, two chains run through the unit cell. That P_5V_4 has a similar structure becomes evident when we neglect the differences between the two

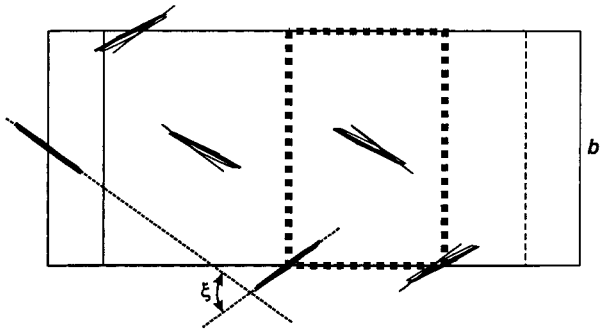

Figure 5. Projection of the unit cell of P_5V_4 along the long molecular axes. If all six molecules were identical, the projected unit cell would reduce to one containing just two molecules and its footprint would be given by the dotted rectangle occupying one-third of the *ab* surface area. ξ is the herringbone angle for the centrosymmetric molecules.

crystallographically distinct molecules and focus on the projections of the molecules along their long axes. The unit cell then reduces to one-third of its actual size, comprising two molecules in the herringbone arrangement (Figure 5). This correspondence prompts a further comparison between PPV and P_5V_4.

The pioneering work on the structure of PPV has been carried out in the mid-1980s by research groups in Amherst[30] and Cambridge.[32] Granier et al.[30] based their model on electron diffraction data obtained on highly oriented (draw ratio 20) films of precursor-route PPV. The main features are sketched in Figure 8. (For comparison with P_5V_4, we have interchanged the designation of *a*- and *b*-axes that was used by Granier et al. for PPV.)

The long axes of the P_5V_4 molecules are highly parallel to the *ac*-plane, but there is a distinct angle between the molecular axis and the *c*-axis (Figure 6). If the crystal structure of the oligomer were to tend toward that of the polymer, this angle should be such that one molecule lines up with another. (In the polymer crystal, the chain is along a unit cell axis by the requirement of translational symmetry.) In the somewhat complicated cell of P_5V_4, only a zero angle would lead to the proper alignment; the actual angle is 3.5°. Remarkably, the length of 33 Å found for the *c*-axis of the oligomer crystal corresponds closely to the length of five repeat units in PPV (c = 6.6 Å). (In the oligomer crystal, five repeat units would be obtained by replacing the terminal H atoms by one −CH═CH− link. The distance between the nearest end atoms of two *c*-axis neighbor molecules, e.g., C3−C36($x,y,z+1$) = 3.81 Å and H3−H36($x,y,z+1$) = 2.41 Å, is almost right. If we carry out this chemistry in a *gedankenexperiment*, changing the chemical composition from to $C_{38}H_{30}$ to $(C_8H_6)_5$ while retaining the cell volume, the calculated density becomes 1.311 g cm^{-3} at 220 K or 1.290 g cm^{-3} at room temperature. The latter compares well to a density of 1.283 g cm^{-3} for PPV.[30])

In oligo(*p*-phenylene)s, the axis of the molecule aligns more and more along the long cell axis as the length of the oligomer increases, with the notable exception of sexiphenyl, however.[24] Polymorphism was suggested as a possible cause of this anomaly. The coexistence of two phases with slightly different cell parameters has indeed been reported for thin films,[33] but a detailed description of a second crystal structure of sexiphenyl is still lacking. Such data would be relevant, since the studies of optical and optoelectronic properties of oligo(*p*-phenylene)s have almost exclusively been limited to thin films of the hexamer.[34]

(25) Bondi, A. *J. Phys. Chem.* **1964**, *68*, 441−451.
(26) Spek, A. L. *Acta Crystallogr.* **1990**, *A46*, C-34.
(27) Bott, D. C.; Brown, C. S.; Winter, J. N.; Barker, J. *Polymer* **1987**, *28*, 601−616.
(28) Sasaki, S.; Yamamoto, T.; Kanbara, T.; Morita, A.; Yamamoto, T. *J. Polym. Sci., Part B: Polym. Phys.* **1992**, *30*, 293−297.
(29) Brückner, S.; Porzio, W. *Makromol. Chem.* **1988**, *189*, 961−967.
(30) Granier, T.; Thomas, E. L.; Gagnon, D. R.; Karasz, F. E.; Lenz, R. W. *J. Polym. Sci., Part B: Polym. Phys.* **1986**, *24*, 2793−2804.
(31) Kavesh, S.; Schultz, J. M. *J. Polym. Sci. A-2* **1970**, *8*, 243−276.
(32) Bradley, D. D. C. *J. Phys. D: Appl. Phys.* **1987**, *20*, 1389−1410.
(33) Athouël, L.; Riou, M. T.; Froyer, G.; Louarn, G.; Lefrant, S.; Siove, A.; Chevrot, C. *J. Chim. Phys.* **1992**, *89*, 1271−1277.

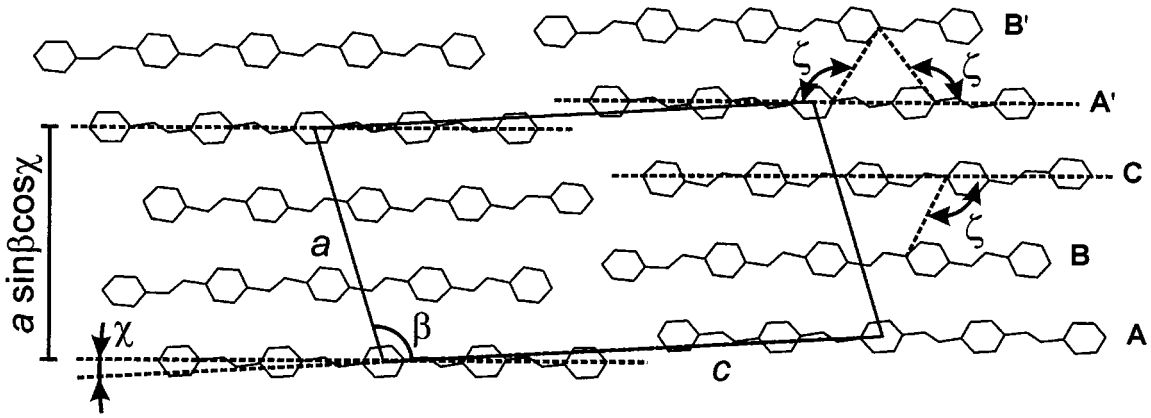

Figure 6. Projection of molecules in one layer onto the *ac*-plane. χ is the angle between the molecular axis (e.g. C41−C44a) and the *c*-axis. The separation between neighbor molecular axes is ($a \sin \beta \cos \chi$)/3. Shift angles ζ between symmetry-related (B, C) and unrelated (A′, B′) molecules are indicated.

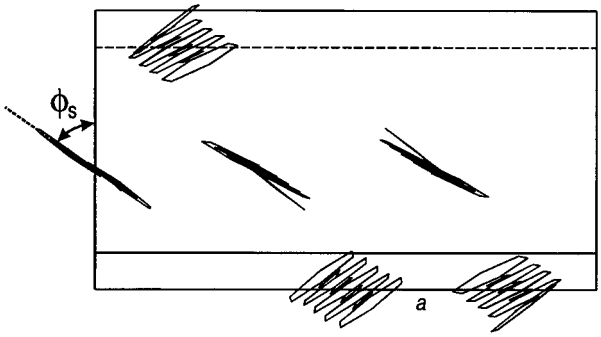

Figure 7. Projection along the intersection of the molecular plane and the *bc*-plane. The setting angle ϕ_s is defined as indicated.

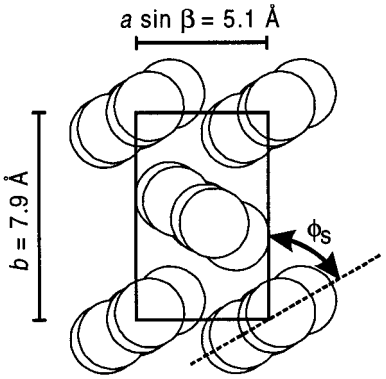

Figure 8. Structure of PPV according to the data by Granier et al.[30] Projection of the unit cell along *c* (chain axis direction) on a perpendicular plane. Crystal data: $a = 6.05$ Å, $b = 7.90$ Å, $c = 6.58$ Å, and $\beta = 123°$.

In both PPV and P_5V_4, molecules with identical orientation of the conjugated plane are most closely packed in the *ac*-plane. In PPV, these chains are equivalent but shifted along their long axis, and their distance is most straightforwardly defined in the projection onto a plane orthogonal to the *c*-axis and given by $a \sin \beta = 5.1$ Å (Figure 8). In P_5V_4, the arrangement of neighbors in the *ac*-plane is very similar. The value of $a \sin \beta$ equals 15.64 Å, reflecting that neighbor molecules are not equivalent and full translational symmetry is found for every third neighbor along *a* (Figure 6, note that the ends of the molecules are arranged in a saw-tooth pattern and that the vinylene bonds are inclined in a ...\ // \ //... pattern in this view). The distance between neighbors is therefore found as ($a \sin \beta$)/3 = 5.2 Å (measuring the distance perpendicular to the molecular axis instead of *c* introduces a factor of $\cos \chi = 0.998$). The lengths of the *b*-axes can be directly compared: the values are 7.6 Å for P_5V_4 and 7.9 Å for PPV.

The axial shift between neighboring molecules is clearly driven by packing constraints that strive to have bulky phenylene groups surrounded by less demanding vinylene groups. This shift causes the unit cell to be monoclinic rather than orthorhombic, and the amount of shift is directly connected to the value of the monoclinic angle. In PPV, a value of 123° is proposed by Granier et al.,[30] although with limited accuracy. The later study by Chen et al.[35] has confirmed these earlier results. In our P_5V_4 crystal, the monoclinic angle β deviates much less from 90°, due to the larger value of *a*. Still, the packing in the *ac*-plane is similar, and picking "equivalent" atoms on neighbor molecules to define an axial shift leads to an angle ζ in the range 115−130° (depending on the molecules and atoms chosen; Figure 6).

In the context of π-conjugation, the dihedral angles between successive phenylene and vinylene units are of interest. Chen et al.[35] have estimated a value of 10 ± 3° for PPV. In P_5V_4, these dihedrals are found to vary between 2° and 12° (with 0.5−0.9° uncertainty). Hence, with regard to conjugation, the oligomer can be considered planar. The noncentrosymmetric molecule has one end ring which deviates markedly from the average plane; it makes an angle of 7° with the penultimate ring (5° in the slightly less accurate analysis at 293 K). Other than that, the angles between the planes of successive rings are below 2°, with 2° uncertainty (the maximum values at 293 K are about 1° higher). A neutron diffraction study by Mao et al.[36] has provided a more detailed picture for PPV in which librational motions of the phenylene rings over 7° are superposed on phenylene-to-vinylene dihedrals of approximately 8°.

The "setting" angle, ϕ_s, of the molecular plane against the *bc*-plane was estimated to be in the range 56−68° by Granier et al.,[30] and around 50° by Chen et al.[35] (Figure 8). Neutron diffraction data from deuterated PPV, which are more sensitive toward the position of the phenylene rings, put the value of ϕ_s at 54°.[36] The setting angle is 55° for the centrosymmetric molecule in the cell of P_5V_4 (Figure 7).

We note that the similarity between the structure of P_5V_4 and the structural model for PPV put forward by Granier et al., based on limited data, suggests that the latter is basically correct.

(34) Piaggi, A.; Lanzani, G.; Bongiovanni, G.; Mura, A.; Graupner, W.; Meghdadi, F.; Leising, G.; Nisoli, M. *Phys. Rev. B* **1997**, *56*, 10133−10137.

(35) Chen, D.; Winokur, M. J.; Masse, M. A.; Karasz, F. E. *Polymer* **1992**, *33*, 3116−3122.

(36) Mao, G.; Fischer, J. E.; Karasz, F. E.; Winokur, M. J. *J. Chem. Phys.* **1993**, *98*, 712−716.

Thermal Expansion. From the cell parameters obtained at the two temperatures of measurement we derive a first, crude approximation of the linear thermal expansion coefficients, α, along the cell axes *b* and *c* and along the direction orthogonal to both *b* and *c*: $\alpha_b = 1.46(5) \times 10^{-4}$; $\alpha_c = 3.1(4) \times 10^{-5}$; and $\alpha_{\perp bc} = 5.1(4) \times 10^{-5}$ (a constant value of α is assumed over this temperature range and the cell axis values at 293 K are chosen as the reference values.) Expansion decreases in the order $\alpha_b > \alpha_{\perp bc} > \alpha_c$. Data on the expansion of the lattice of PPV over the range 20−700 K were published by Chen et al.[35] From their data we estimate a room temperature linear expansion coefficient of about 7×10^{-5} perpendicular to the chain axis; the value rises with temperature. The neutron diffraction data by Mao et al.[36] more conclusively demonstrate anisotropy and reveal an increase in the ratio $b/(a \sin \beta)$ by 0.015 between 296 and 616 K. For our oligomer crystal, the ratio $3b/(a \sin \beta)$ changes from 1.4461(3) at 220 K to 1.4562(7) at 293 K. The rate of change thus appears to be higher in the case of P_5V_4. The issue here is whether the axial ratio progresses toward a more hexagonal structure (ratio $\sqrt{3}$) in which each molecule is cylindrically symmetric around its long axis at high temperature (like the "rotator phase" of alkanes, also proposed for polyethylene[37]). Such a structural evolution could be associated with the occurrence of a liquid-crystalline phase, as suggested by the DSC data for P_5V_4 presented above. Mao et al.,[36] however, argue that this evolution is unlikely because independent librational motions of the phenylene rings are a major degree of freedom, suppressing the concerted chain motion necessary for conformational changes.

Substituents, Molecular Packing, and Transport in Conjugated Oligomers. We have synthesized and investigated a variety of three-ring, five-ring, and even larger oligomers of phenylenevinylene-type. Most of the three- and five-ring oligomers have been obtained as single crystals suitable for X-ray analysis. The results of the crystallographic studies so far showed that none of the compounds that bear substituents on the central ring display a herringbone-type molecular packing in the crystal. Some have a $P\bar{1}$ cell (with one centrosymmetric molecule), others have two or more molecules per cell, but in those cases the axes of the conjugated backbones are not parallel. Herringbone packing is apparently not compatible with the presence of laterally attached substituents; these cannot be accommodated efficiently. The structure of the methoxy-substituted three-ring oligomer may serve as an illustration (Figure 9). Even though the methoxy group is small, the packing is entirely different from herringbone; the individual molecules are very nonplanar as well. Unfortunately, the structure of unsubstituted P_3V_2 is not known. (In crystals of *trans*-stilbene, the axes of the two molecules in the cell are far from parallel;[38,39] this may be attributed to the small aspect ratio of the molecule.)

The effects of substituents on the electronic state of single molecules as well as on optical properties of the solid state have been investigated for some OPVs, primarily substituted P_3V_2s.[40,41] The structure of the crystalline phase has only occasionally been considered in these studies. Le Rendu et al.[42] reported on the electrical properties of a vapor-deposited film of P_5V_4 synthesized by the Wittig route. Their P_5V_4 is reported to be a bright yellow powder, but there is no further characterization of the solid in terms of structure or morphology. A more favorable case is represented by α-sexithiophene (α6T), where the relation between structure and transport properties has been extensively studied in the context of applications in transistor and photovoltaic devices. In films of unsubstituted α6T, Servet et al.[43] found polymorphism, a strong dependence on the deposition conditions (i.e., substrate temperature and deposition rate) of both the type of crystal structure and the morphology obtained. Field-effect mobility as well as the value and anisotropy of the dc conductivity were found to vary sensitively with the structure. Deposition at room temperature may produce a film containing crystallites with molecules parallel as well as those with molecules perpendicular to the substrate. Alkyl substitution of the α,ω-type, i.e., at the terminal hydrogen positions of the molecule, induces a much increased structural regularity of films obtained at room temperature, as compared to α6T.[3] In films of α,ω-dihexylsexithiophene, the orientation of the molecules is uniform with the long axis nearly perpendicular to the substrate. The dissimilarity between the alkyl group and the conjugated backbones induces in the molecule the tendency to structured self-assembly, which is directly reflected in superior transport properties. The measured quantities, however, still represent the composite effects of crystallographic order and morphology (nature and density of grain boundaries). For α6T substituted with hexyl groups in the β-position on both terminal rings, conductivity and mobility values were found to be about 6 orders of magnitude lower.[3] This may be readily attributed to a larger separation between conjugated systems due to the lateral substituents, but it should be noted that this β-substituted α6T was not regioregular, and the crystallographic order appeared to be very poor. (Regioregular β-substitution of α6T, on the other hand, has led to the formation of single crystals in several cases.[44,45])

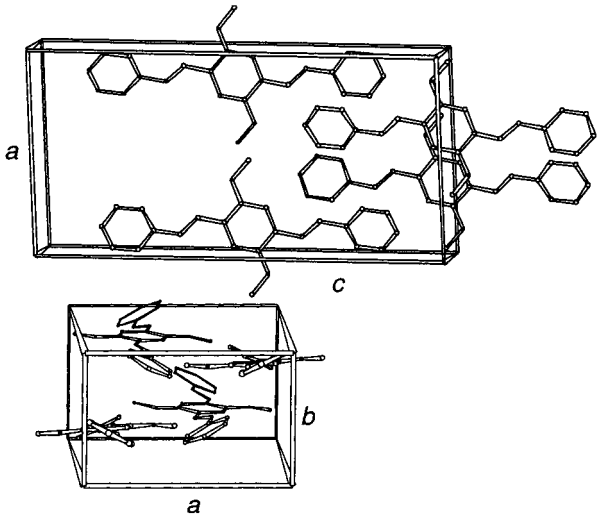

Figure 9. Molecular packing of methoxy-substituted P_3V_2. The four molecules that make up one unit cell are shown, viewed perpendicular to the plane of the central ring (top), and at a slight angle with respect to the long molecular axes (bottom). Crystal data: $P2_1/n$, $a = 11.213$ Å, $b = 7.164$ Å, $c = 22.317$ Å, and $\beta = 92.736°$.

(37) Strobl, G.; Ewen, B.; Fischer, E. W.; Piesczek, W. *J. Chem. Phys.* **1974**, *61*, 5257−5264.
(38) Finder, C. J.; Newton, M. G.; Allinger, N. L. *Acta Crystallogr.* **1974**, *B30*, 411−415.
(39) Bouwstra, J. A.; Schouten, A.; Kroon, J. *Acta Crystallogr.* **1984**, *C40*, 428−431.
(40) Stalmach, U.; Detert, H.; Meier, H.; Gebhardt, V.; Haarer, D.; Bacher, A.; Schmidt, H.-W. *Opt. Mater.* **1998**, *9*, 77−81.
(41) Oelkrug, D.; Tompert, A.; Gierschner, J.; Egelhaaf, H.-J.; Hanack, M.; Hohloch, M.; Steinhuber, E. *J. Phys. Chem. B* **1998**, *102*, 1902−1907.
(42) Le Rendu, P.; Nguyen, T. P.; Gaudin, O.; Tran, V. H. *Synth. Met.* **1996**, *76*, 187−190.
(43) Servet, B.; Horowitz, G.; Ries, S.; Lagorsse, O.; Alnot, P.; Yassar, A.; Deloffre, F.; Srivastava, P.; Hajlaoui, R.; Lang, P.; Garnier, F. *Chem. Mater.* **1994**, *6*, 1809−1815.
(44) Herrema, J. K.; Wildeman, J.; Van Bolhuis, F.; Hadziioannou, G. *Synth. Met.* **1993**, *60*, 239−248.

Table 3. Electrical Properties and Efficiencies of Single-Layer OPV-LEDs with ITO Hole-Injecting Contacts in Forward-Bias Operation; Estimated HOMO−LUMO Gaps and Hole Injection Barriers (ϕ_{holes}) for the OPVs

compd	film type[a]	cathode	film thickness[b] (nm)	$V_{turn-on}$[c] (V)	$E_{turn-on}$ (10^8 V m^{-1})	external eff (10^{-4} ph/el)	HOMO−LUMO gap[d] (eV)	ϕ_{holes}[e] (eV)
P_5V_4	as	Al	380	18.1	0.5	1.1	2.7	0.2
$Oct_2P_5V_4$	as	Al	193	24.4	1.3	0.1	2.4	0.2
	an	Al		20.4	1.1	1.2		

[a] As: LED with film as-deposited. An: LED annealed at 120 °C. [b] Film thickness was measured with a Dektak 3130 surface profiler. [c] Turn-on is defined here as the point at which the emission is detectable. [d] From optical absorption measurements. [e] From Fowler−Nordheim analysis.

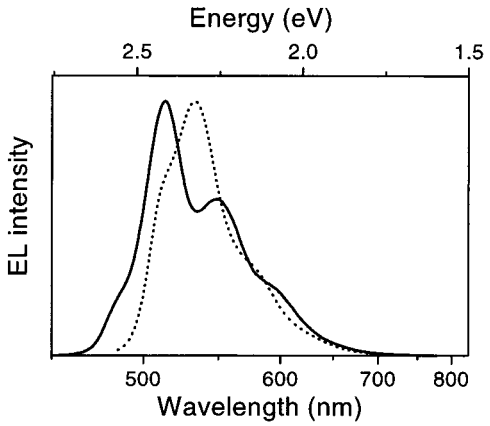

Figure 10. Normalized electroluminescence spectra of ITO/OPV/Al devices: P_5V_4 (—) and $Oct_2P_5V_4$ (· · ·).

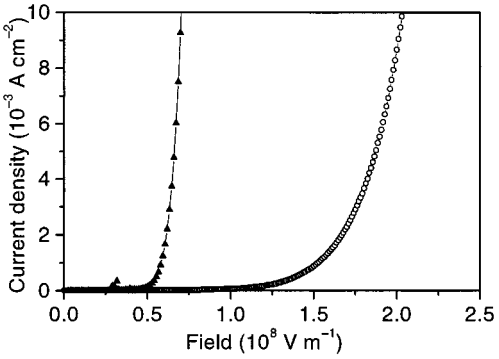

Figure 11. Electrical characteristics of ITO/OPV/Al devices: P_5V_4 (▲) and $Oct_2P_5V_4$ (○).

Electroluminescence. A first impression of the optoelectronic properties of P_5V_4 was obtained from measurements on single-layer ITO/OPV/Al LEDs. These were prepared as described in the Experimental Section, for P_5V_4 and $Oct_2P_5V_4$.[46] The electroluminescence (EL) spectra of the single-layer devices are depicted in Figure 10. For these OPVs, EL spectra coincide with the solid-state photoluminescence spectra, indicating that the same excited states are involved in both PL and EL. The spectrum from P_5V_4 has its maximum at 2.4 eV, and the absorption edge is found around 2.7 eV. These values are approximately 0.2 eV blue-shifted relative to the spectrum of unsubstituted PPV,[47] indicating that the effective conjugation length of PPV exceeds that of P_5V_4 . EL from $Oct_2P_5V_4$ is red-shifted relative to P_5V_4 due to the electron-donating effect of the octyloxy substituents.

The efficiency values (Table 3) are significantly higher than those of single-layer LEDs prepared from substituted oligothiophenes and are comparable to LED efficiencies for PPV-based polymers. The minimum thickness of the active layer must be around 150 nm or more to obtain reproducible diode characteristics. The current−voltage characteristics are shown in Figure 11. All diodes showed rectifying behavior and we did not observe electroluminescence in reverse bias for any of these devices. Electrical measurements on devices with different layer thickness have shown that the diode current depends on the applied field rather than the drive voltage. This indicates that field-driven injection determines the electrical characteristics. By means of Fowler−Nordheim analysis of the $I-V$ characteristics and optical absorption measurements, we estimated the injection barrier for holes (ϕ_{holes}) and the HOMO−LUMO gap, respectively.[48] The $I-V$ characteristics are determined by the majority carriers in these devices, which are holes. On the basis of the similar hole-injection barrier for both OPVs, one would expect approximately the same electrical characteristics. However, P_5V_4 has a lower onset for both current and emission, the onset for light emission appearing at half the electric field strength found for $Oct_2P_5V_4$. Moreover, the barrier for electron injection is approximately 0.3 eV higher for P_5V_4 . A possible explanation for the difference in behavior is that the charge carrier mobilities are much higher in the case of P_5V_4, resulting in a higher injection rate of charge carriers.[49] The higher mobility is attributed to the absence of side chains on this molecule, and the resulting closer packing of the π-systems in the solid.

Conclusion and Outlook

The similarity between the generally accepted structural model for PPV and the crystal structure of P_5V_4 found in this work makes it very desirable to investigate the optoelectronic properties of the latter compound in more detail. Studies of the transport properties of several OPVs are currently under way to allow comparisons between solids that have a different molecular packing; these can be either different compounds or (crystallographically or morphologically) different states of the same compound. We are confident that this approach will benefit our understanding of the transfer mechanisms for optical and charged excitations in semiconducting organic materials.

Acknowledgment. We are indebted to Anita Coetzee and Leo Straver of Nonius BV in Delft (The Netherlands) for collection of the X-ray data on their KappaCCD system. Data collection on the Bruker SMART 1000 CCD diffractometer system followed by structure refinement was kindly carried out by Ludger Häming and Michael Ruf of Bruker Analytical X-ray Systems in Karlsruhe (Germany). The authors thank Hendrik-Jan Brouwer and Mathieu Knaven for their experimental contribution in the work on LEDs and Gert Alberda van

(45) Sato, T.; Fujitsuka, M.; Shiro, M.; Tanaka, K. *Synth. Met.* **1998**, *95*, 143−148.

(46) Brouwer, H.-J. Semiconducting polymers for light-emitting diodes and lasers; a structural, photophysical and electrical study of PPV-type alternating copolymers and oligomers; Ph.D. Thesis; Groningen, The Netherlands, 1998.

(47) Burroughes, J. H.; Bradley, D. D. C.; Brown, A. R.; Marks, R. N.; Mackay, K.; Friend, R. H.; Burn, P. L.; Holmes, A. B. *Nature* **1990**, *347*, 539−541.

(48) Parker, I. D. *J. Appl. Phys.* **1994**, *75*, 1656−1666.

(49) Davids, P. S.; Kogan, Sh. M.; Parker, I. D.; Smith, D. L. *Appl. Phys. Lett.* **1996**, *69*, 2270−2272.

Ekenstein for TGA and DSC analyses. This work was financially supported by The Netherlands Organization for Scientific Research (NWO-CW/FOM/STW).

Supporting Information Available: An ORTEP drawing of the non-hydrogen atoms for P_5V_4 and tables of final fractional atomic coordinates, anisotropic thermal parameters for the non-hydrogen atoms, and bond lengths and angles at 220 K. An X-ray crystallographic CIF file is also available. This material is available free of charge via the Internet at http://pubs.acs.org.

JA990934R